Suppression of both superconductivity and structural transition in hole-doped $MoTe_2$ induced by Ta substitution

Siu Tung Lam [1], K. Y. Yip [1], Swee K. Goh [1,*] and Kwing To Lai [1,2,3,†]

[1]*Department of Physics, The Chinese University of Hong Kong, Shatin, Hong Kong, China*
[2]*Shenzhen Research Institute, The Chinese University of Hong Kong, Shatin, Hong Kong, China*
[3]*Faculty of Science, The University of Hong Kong, Pokfulam, Hong Kong, China*

(Received 3 March 2023; accepted 3 August 2023; published 21 August 2023)

Type-II Weyl semimetal $MoTe_2$ exhibits a first-order structural transition at $T_s \sim 250$ K and superconducts at $T_c \sim 0.1$ K at ambient pressure. Both T_s and T_c can be manipulated by several tuning parameters, such as hydrostatic pressure and chemical substitution. It is often reported that suppressing T_s enhances T_c, but our study shows a different behavior when $MoTe_2$ is hole-doped by Ta. When T_s is suppressed by Ta doping, T_c is also suppressed. Our findings suggest that the suppression of T_s does not necessarily enhance superconductivity in $MoTe_2$. By connecting with the findings of electron-doped $MoTe_2$, we argue that varying electron carrier concentration can effectively tune T_c. In addition, the Hall coefficient is enhanced around the doping region, where T_s is completely suppressed, suggesting that the critical scattering around the structural transition may also play a role in suppressing T_c.

DOI: 10.1103/PhysRevMaterials.7.084802

I. INTRODUCTION

Superconductivity is found, often by tuning the electronic properties via the application of hydrostatic pressure, in many topological semimetals, such as Cd_3As_2 [1], $ZrTe_5$ [2], YPtBi [3–6], WTe_2 [7–10], and $MoTe_2$ [11–14]. The exotic combination of topological bands and superconductivity offers a unique platform to search for topological superconductivity, where Majorana fermions can be used to develop topological quantum computation [15,16].

Type-II Weyl semimetal $MoTe_2$ [17–20] is one of the promising candidates for hosting topological superconductivity, especially after the discovery of an edge supercurrent [21]. At ambient pressure, $MoTe_2$ undergoes a first-order structural transition at $T_s \sim 250$ K, changing from a centrosymmetric (nonpolar) monoclinic $1T'$ phase (space group: $P2_1/m$) to a noncentrosymmetric (polar) orthorhombic T_d phase (space group: $Pmn2_1$) on cooling. At $T_c \sim 0.1$ K, an additional superconducting phase transition occurs.

Owing to its low T_c, it is challenging to experimentally study the superconductivity of $MoTe_2$. Finding a suitable way to control its T_c becomes an outstanding issue. Meanwhile, the competition between structural and superconducting transitions in $MoTe_2$ has been reported in previous studies using a variety of tuning parameters. Through the application of pressure [11,13,22–25], T_s is suppressed to 0 K at ~10 kbar, resulting in a complete removal of the T_d phase at high pressures. Meanwhile, T_c is enhanced by 30-fold (~4 K) at ~15 kbar. These behaviors demonstrate the anticorrelation between T_s and T_c. Similar anticorrelation can also be observed via isovalent chemical substitutions (S/Se substituting Te [22,26]) and electron doping (Te deficiency [27] and Re substituting Mo [28]). Note that via the substitution of Mo by W, T_s is enhanced at ambient pressure, and the pressure-induced T_c is lower than that observed in the pristine $MoTe_2$, demonstrating the anticorrelation between T_s and T_c again [29].

The superconductivity of hole-doped $MoTe_2$ has not been studied to the same extent as the electron-doped counterpart. The introduction of hole carriers in monolayer $MoTe_2$ through gating has been shown to reduce its T_c [30]. On the other hand, the effect of hole doping on bulk $MoTe_2$ has been explored in depth through the substitution of Nb for Mo [31,32]. Although no evidence of superconductivity with $T_c > 2$ K has been found up to the highest studied doping level $x = 0.22$ in $Mo_{1-x}Nb_xTe_2$, indicating a lack of significant enhancement in T_c through hole doping, the hole-doping phase diagram of $Mo_{1-x}Nb_xTe_2$ in the normal state was extensively investigated by Sakai *et al.* [32]. They revealed that the suppression of T_s on Nb doping is associated with a huge enhancement of thermopower at low temperatures, which they attributed to the critical scattering arising from the boundary of the nonpolar-to-polar transition around T_s.

Nevertheless, it remains uncertain how T_c evolves and what the correlation of T_s and T_c is on hole doping. Understanding these issues can help us reveal the key factors that control T_c of $MoTe_2$. In this article, we study the effect of hole doping on $MoTe_2$ via the substitution of Mo by Ta. Transport measurements were conducted down to ~30 mK to track the evolution of both T_s and T_c, and surprisingly, we found that both T_s and T_c are suppressed and eventually vanish with increasing hole doping, contrary to the anticorrelation between T_s and T_c established in $MoTe_2$ controlled by other tuning parameters.

*skgoh@cuhk.edu.hk
†ktlai@phy.cuhk.edu.hk

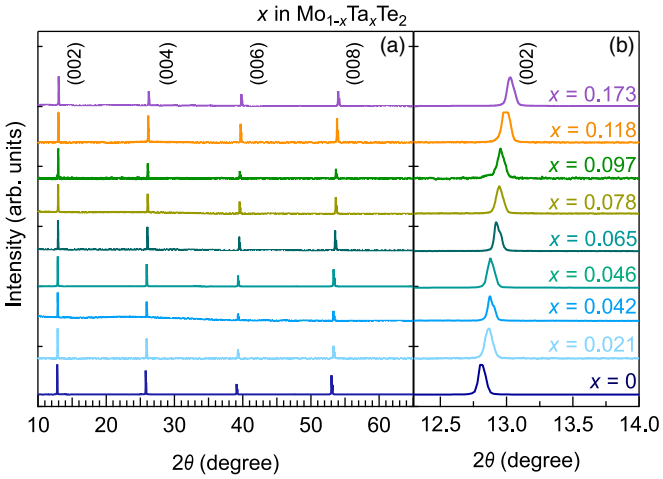

FIG. 1. (a) x-Ray diffraction (XRD) spectra of single crystals of $Mo_{1-x}Ta_xTe_2$. The peaks of (00L) are indexed in the figure. (b) Enlarged XRD spectra near the peak of (002). The (002) peak shifts progressively toward a higher diffraction angle 2θ when x increases.

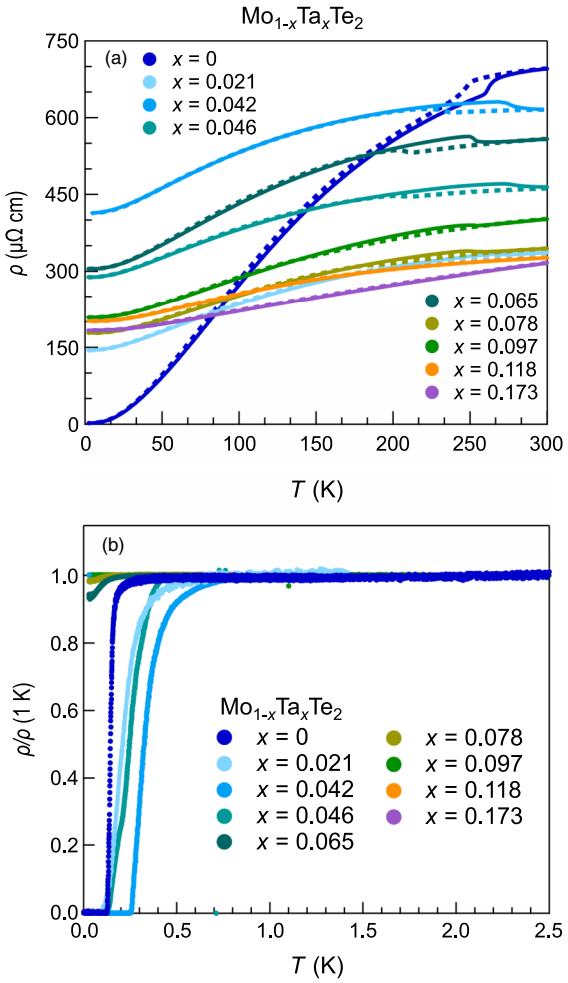

FIG. 2. (a) Temperature dependence of resistivity $\rho(T)$ of $Mo_{1-x}Ta_xTe_2$ at zero magnetic fields. The warm-up (cool-down) data are plotted as solid (dashed) curves. (b) Low-temperature $\rho(T)$ normalized to the value of $\rho(1\,\mathrm{K})$, displaying the superconducting transitions.

II. EXPERIMENT

Single crystals of $Mo_{1-x}Ta_xTe_2$ were grown by the self-flux method. The mixture of Mo powder (99.999%, Alfa Aesar), Te (99.99999% lumps, Ultimate Material), and Ta powder (99.99%, Sigma Aldrich) were first placed into an alumina crucible, with a stoichiometric ratio of Mo:Ta:Te = $1-x$:x:20. The alumina crucible was inserted into a quartz tube before the quartz tube was sealed under a vacuum. The sealed ampule was then heated to 1100 °C within 24 h and stayed for 24 h, followed by slow cooling to 880 °C for 400 h. Finally, the ampule was taken out from the furnace at 880°C and centrifuged to remove the excess Te flux. X-ray diffraction (XRD) data were collected at room temperature by using a Rigaku x-ray diffractometer with CuK_α radiation. The chemical compositions were characterized by a JEOL JSM-7800F scanning electron microscope equipped with an Oxford energy-dispersive x-ray (EDX) spectrometer. A standard four-probe method was used to measure temperature-dependent resistance in a Bluefors dilution refrigerator with a base temperature of 30 mK. A standard six-probe method was used to measure the Hall effect in a Quantum Design Physical Property Measurement System with a temperature range from 300 K to 2 K and a magnetic field of ±14 T.

III. RESULTS AND DISCUSSION

Figure 1(a) shows the XRD spectra for the $Mo_{1-x}Ta_xTe_2$ single crystals with $x = 0$, 0.021, 0.042, 0.046, 0.065, 0.078, 0.097, 0.118, and 0.173. The peaks shown in all spectra are well indexed by the (00L) planes originating from the pattern of $1T'$-$MoTe_2$, confirming that all crystals are single-crystalline $1T'$-$MoTe_2$ at room temperature. Figure 1(b) focuses on the (002) peaks of all samples, which reveal a monotonic shift to a higher 2θ when x increases, indicating a shrinking crystal structure. As the covalent radius of Ta is smaller than that of Mo, this provides crystallographic evidence that Ta is systemically substituting Mo with increasing x. These $Mo_{1-x}Ta_xTe_2$ crystals measured in XRD were also examined by EDX, from which we determined their elemental compositions and hence the values of x in each sample. The EDX results are consistent with the findings in XRD spectra (see the Supplemental Material for more details [33]).

Figure 2(a) illustrates the temperature dependence of resistivity $\rho(T)$ of $Mo_{1-x}Ta_xTe_2$ with $x = 0$–0.173 measured under zero magnetic field. All samples exhibit metallic behavior. A thermal hysteresis can be observed in pristine $MoTe_2$ ($x = 0$) around 150–250 K when the resistivity was measured on increasing (solid curves) and decreasing temperature (dashed curves), indicating the appearance of the first-order structural transition [11,13,14,34,35]. This transition persists up to $x = 0.097$. With increasing x, the transition shifts gradually toward lower temperatures, and the hysteresis loop becomes broader. When $x \geqslant 0.118$, no hysteresis is observed in the whole temperature range, suggesting that the structural transition vanishes at the high-doping region. Figure 2(b) shows the resistivity data normalized to the value of $\rho(T)$ at 1 K at the low-temperature region. A supercon-

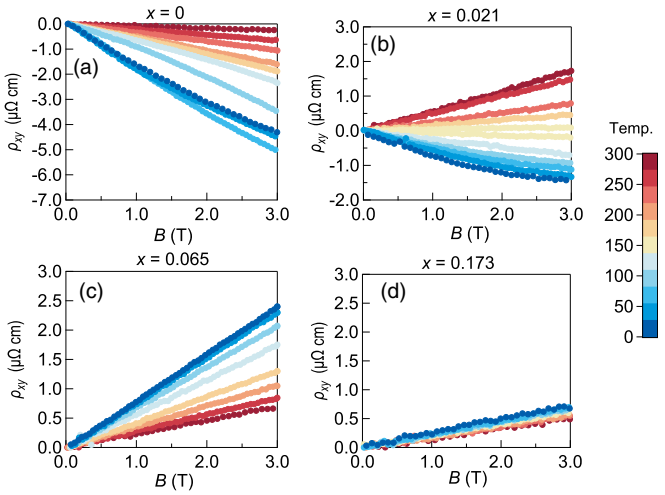

FIG. 3. Magnetic field dependence of Hall resistivity $\rho_{xy}(B)$ of $Mo_{1-x}Ta_xTe_2$ with (a) $x = 0$, (b) $x = 0.021$, (c) $x = 0.065$, and (d) $x = 0.173$ collected during warm-up. The color scale at the right indicates the measured temperature.

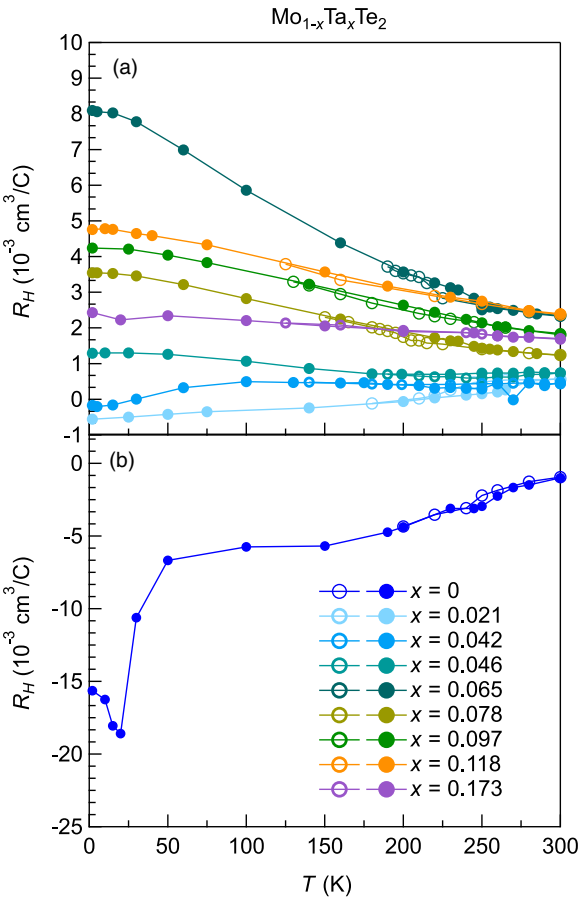

FIG. 4. Temperature dependence of Hall coefficient R_H of (a) $Mo_{1-x}Ta_xTe_2$ with $x \neq 0$ and (b) pristine $MoTe_2$ ($x = 0$). The closed (open) symbols represent the warm-up (cool-down) data. The cool-down data are only shown at high temperatures.

ducting transition, where T_c is defined at which the resistivity drops to zero, is observed at $x = 0$ with $T_c \sim 0.1$ K, which is consistent with the previous studies [11–14,21–25,35]. When x increases, T_c generally reduces despite a small enhancement to ~0.25 K at $x = 0.042$. At $x = 0.065$, a small drop of resistivity without reaching zero resistivity is observed near the base temperature, indicating that the bulk superconductivity is heavily suppressed and only trace superconductivity is detected. When x further increases ($\geqslant$0.078), the resistivity data shows no signs of superconductivity.

To probe the evolution of the Fermi surface of $Mo_{1-x}Ta_xTe_2$, we conducted the Hall effect measurements. Figure 3 illustrates the magnetic field dependence of Hall resistivity $\rho_{xy}(B)$ of $Mo_{1-x}Ta_xTe_2$ with $x = 0$, 0.021, 0.065, and 0.173 at different temperatures measured during warm-up. $\rho_{xy}(B)$ data of samples with other doping can be found in Fig. S2 in Supplemental Material [33]. At $x = 0$ [Fig. 3(a)], $\rho_{xy}(B)$ has a negative slope at the whole temperature range. At low temperatures, $\rho_{xy}(B)$ shows a nonlinear feature. These features are consistent with the semimetallic nature of $MoTe_2$, which exhibits nearly perfect electron-hole compensation with a high electron mobility [13,36]. After introducing Ta doping, the slope of $\rho_{xy}(B)$ at $x = 0.021$ [Fig. 3(b)] begins to turn positive at high temperatures. When x further increases, the slope is always positive at all measured temperatures [see Figs. 3(c) and 3(d) as examples]. This trend indicates that Ta doping introduces hole carriers to the samples and the hole carriers are dominant at $x > 0.021$. Moreover, the additional hole carriers destroy the nearly perfect electron-hole compensation, resulting in the linear positive slope of $\rho_{xy}(B)$ at $x > 0.021$.

To further visualize the temperature evolution of the Hall effect of $Mo_{1-x}Ta_xTe_2$, we extract the Hall coefficient R_H from the slope of $\rho_{xy}(B)$ in the linear region, and the temperature evolution of R_H is plotted in Fig. 4. The R_H data measured at high temperatures during cool-down are also displayed. We find that a thermal hysteresis can also be observed in the R_H data of the samples from $x = 0$ to $x = 0.097$, while the hysteresis is absent in the sample with $x \geqslant 0.118$. These results are consistent with the observation of the first-order structural transition in the $\rho(T)$ data in Fig. 2(a). At $x = 0$ [Fig. 4(b)], R_H shows a strong temperature dependence below 50 K, which is similar to the result reported in previous studies [34,36]. On Ta doping, R_H shifts toward the positive side due to the introduction of additional hole carriers, while the temperature dependence is relatively mild compared to $x = 0$. The most prominent temperature profile of R_H in Ta-doped samples is $x = 0.065$, where the magnitude of R_H ($|R_H|$) gradually increases with decreasing temperature and reaches the maximum value at 2 K. Interestingly, our results show that $|R_H|$ at 2 K is the largest around $x = 0.065$ [see also Fig. 3(c), where $\rho_{xy}(B)$ has a steeper slope at 2 K compared to that in Fig. 3(d)], which is different from the expectation that R_H would increase toward the positive side when x increases. This issue will be further discussed in the later section.

We summarize our results and construct a temperature-doping phase diagram of $Mo_{1-x}Ta_xTe_2$ in Fig. 5, which shows the Ta-doping dependence of T_s and T_c. The structural transition temperatures acquired during warm-up ($T_{s,\mathrm{warm}}$) and cool-down ($T_{s,\mathrm{cool}}$) are defined by the extrema of the first derivative of $\rho(T)$ around the transition (see Fig. S3 in the

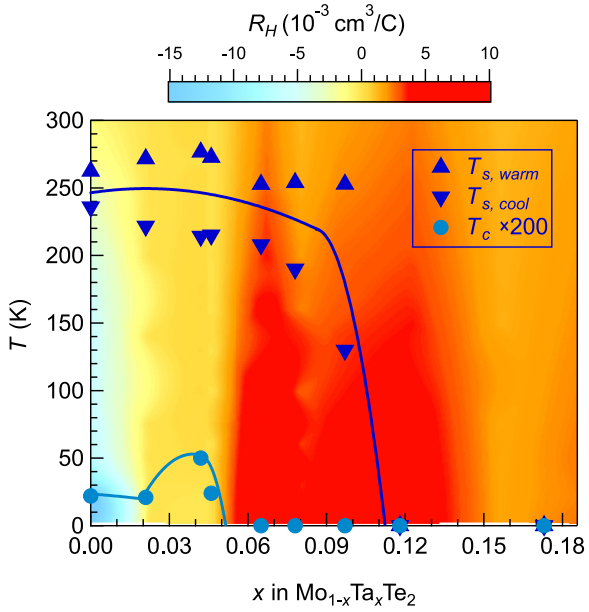

FIG. 5. Temperature-doping phase diagram of $Mo_{1-x}Ta_xTe_2$. The upward (downward) blue triangles represent T_s defined from the temperature-dependent resistivity data measured during warm-up (cool-down). The solid cyan circles represent T_c. The solid curves are guides for the eyes. The color contour denotes the temperature dependence of Hall coefficient R_H at different doping levels.

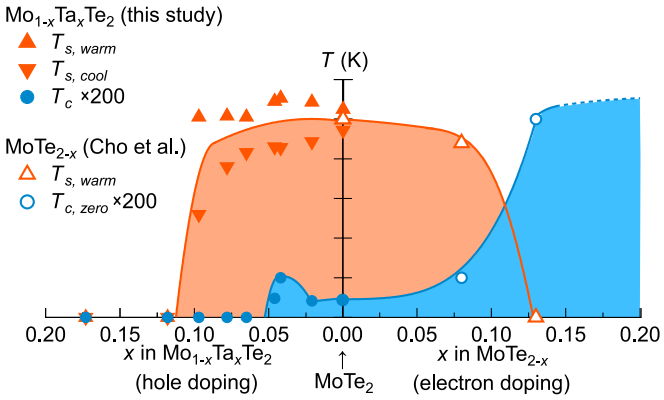

FIG. 6. Temperature-doping phase diagram of hole-doped and electron-doped $MoTe_2$. The hole-doping data (solid symbols) are our findings of $Mo_{1-x}Ta_xTe_2$, as shown in Fig. 5, while the electron-doping data (open symbols) are adapted from the findings of Te-deficient $MoTe_{2-x}$ from Cho *et al.* [27].

Supplemental Material [33]). Both $T_{s,\,\mathrm{warm}}$ and $T_{s,\,\mathrm{cool}}$ show a generally decreasing trend with increasing x. Compared to $T_{s,\,\mathrm{warm}}$, $T_{s,\,\mathrm{cool}}$ decreases more rapidly with increasing x. When $x \geqslant 0.118$, both $T_{s,\,\mathrm{warm}}$ and $T_{s,\,\mathrm{cool}}$ are completely suppressed. On the other hand, after experiencing a local maximum at $x = 0.042$, T_c also decreases when x increases and drops to zero at $x \geqslant 0.065$ (before T_s vanishes). The disappearance of superconductivity is unique in our hole-doping phase diagram; in the previous phase diagram studies of $MoTe_2$ on pressure [11,13,22–25], isovalent chemical substitution [22,26], and electron doping [27,28], they typically show the anticorrelation of T_c and T_s as well as a huge enhancement of T_c.

To shed light on the issue of why the superconductivity of $MoTe_2$ is suppressed on hole doping, a contour plot of R_H is overlaid in Fig. 5. We reveal that $|R_H|$ is significantly enhanced around the region when T_s is suppressed to zero ($x \sim 0.1$), and T_c vanishes when the enhancement of $|R_H|$ emerges at $x \sim 0.05$. Compared to the previous studies with other tuning parameters, while T_c increases, low-temperature $|R_H|$ has either a weak electron-doping dependence [27,28] or decreases with pressure [13]. Meanwhile, a similar enhancement of R_H has been observed in another hole-doping study, Nb-doped $MoTe_2$ [32]. Such enhancement is associated with the enhancement of thermopower divided by temperature S/T, which is maximum around the region where T_s is completely suppressed; our R_H contour plot is reminiscent of the contour plot of S/T reported in the phase diagram of Nb-doped $MoTe_2$ (Fig. 1(b) in Ref. [32]). According to Sakai *et al.*'s argument, both enhancements of R_H and S/T are attributed to the strong fluctuation or phase separation around the nonpolar-polar structural transition, giving rise to some critical scattering effects on the carriers [32]. Combining this statement with our phase diagram, the critical scattering may also hinder the formation of Cooper pairs, and therefore suppress superconductivity. Further investigations on the competition between superconductivity and critical scattering are highly desired to confirm this picture.

Another possible explanation for the suppression of superconductivity is related to the change in the Fermi surface topology on hole doping. Cho *et al.* [27] have performed theoretical calculations on the impact of electron and hole doping on T_c. While they have attributed the increase in T_c on electron doping (arising from Te vacancy in $MoTe_{2-x}$) to the enhancement of the density of states at the Fermi level [$N(E_F)$] and the electron-phonon coupling constant (λ), they have also predicted that, on hole doping, $N(E_F)$ and λ will be suppressed and therefore T_c will decrease, which is consistent with our experimental findings. Cho *et al.* further attributed the change in λ to phonon vectors connecting between electron Fermi pockets, which are enlarged on electron doping according to their calculations. In contrast, on hole doping, electron pockets shrink and only spherical-shaped hole pockets remain at the Γ point [27,32]. In the situation without phonon vectors linking between electron pockets, λ will be suppressed and hence T_c will be reduced. Therefore, our study has provided solid experimental evidence to showcase Cho *et al.*'s theoretical prediction.

To further elaborate on this idea, we connect our hole-doping phase diagram with the electron-doping phase diagram (based on the result of Te-deficient $MoTe_2$ from Cho *et al.* [27]) and plot the combined phase diagram in Fig. 6. It unambiguously shows the asymmetry between the hole-doping phase and electron-doping diagrams, which is reminiscent of different behaviors between hole-doped and electron-doped cuprate superconductors [37,38]. While T_s shows a similar suppression on both hole and electron doping, the doping dependence of T_c behaves differently. At the electron-doping region (the right-hand side of Fig. 6), T_c is largely enhanced. However, when we move to the hole-doping region (the left-hand side of Fig. 6), T_c is heavily suppressed. This demonstrates a clear trend that T_c can be induced and enhanced when

the electron carrier concentration increases, no matter what the phase is.

Meanwhile, although the critical scattering around the structural transition may contribute to the suppression of superconductivity, our result shows that the tuning of the carrier concentration, which controls the phonon nesting vector(s), provides an effective means to vary the T_c of $MoTe_2$, regardless of the suppression of T_s. These findings provide experimental evidence that enhancing the T_c of $MoTe_2$ by solely increasing the electron carrier concentration while preserving the topologically nontrivial T_d phase is possible. Such property can potentially boost the progress of the search for topological superconductivity in $MoTe_2$, which is currently hindered by its low T_c.

IV. CONCLUSIONS

In summary, we have investigated the phase diagram of Ta-doped $MoTe_2$, $Mo_{1-x}Ta_xTe_2$, with $x = 0-0.173$ through magnetotransport measurements. Single crystals of $Mo_{1-x}Ta_xTe_2$ were successfully grown by the self-flux method. x-Ray diffraction and energy-dispersive x-ray spectroscopy have confirmed that Mo is partially substituted by Ta in the doped samples. By measuring the temperature dependence of resistivity and the Hall effect, we have revealed that the structural transition temperature T_s is completely suppressed at $x \sim 0.11$, while the superconducting transition T_c generally decreases on Ta doping and finally vanishes at $x \sim 0.08$. This behavior is in contrast to the previous phase diagrams constructed based on applying pressure, isovalent doping, or electron doping, which show the enhancement of T_c when T_s is suppressed. Moreover, the Hall coefficient is found to be enhanced at low temperatures around the region where T_s is suppressed to zero, suggesting that the critical scattering arising from the structural temperature may have some contributions to the suppression of T_c. By comparing our findings with the phase diagram of electron-doped $MoTe_2$, we argue that the electron carrier concentration in $MoTe_2$ is a key factor in controlling T_c, which offers a straightforward way to boost the T_c of $MoTe_2$.

Note added. After the first submission of this article, we noticed a recently published article [39] which reports an enhancement of T_c in Ta-doped $MoTe_2$. Our results do not agree with those of Ref. [39]. The discrepancy may be attributed to methodological differences. First, Ref. [39] used a different crystal growth condition. Second, we determine our T_c values based on the observation of zero resistivity while Ref. [39] deduced their T_c values from the onset of the transition in resistivity. We note that zero resistivity has not been observed in the doped samples in Ref. [39].

ACKNOWLEDGMENTS

We acknowledge Xinyou Liu, Ying Kit Tsui, Wei Zhang, and Lingfei Wang for fruitful discussions, and financial support from the Research Grants Council of Hong Kong (Grants No. GRF/14300419, No. GRF/14301020, and No. A-CUHK402/19), CUHK Direct Grant (Grants No. 4053463, No. 4053528, No. 4053408, and No. 4053461), and the National Natural Science Foundation of China (Grant No. 12104384).

[1] L. He, Y. Jia, S. Zhang, X. Hong, C. Jin, and S. Li, Pressure-induced superconductivity in the three-dimensional topological Dirac semimetal Cd_3As_2, npj Quant. Mater. **1**, 16014 (2016).

[2] Y. Zhou, J. Wu, W. Ning, N. Li, Y. Du, X. Chen, R. Zhang, Z. Chi, X. Wang, X. Zhu, P. Lu, C. Ji, X. Wan, Z. Yang, J. Sun, W. Yang, M. Tian, Y. Zhang, and H.-k. Mao, Pressure-induced superconductivity in a three-dimensional topological material $ZrTe_5$, Proc. Natl. Acad. Sci. USA **113**, 2904 (2016).

[3] M. Meinert, Unconventional Superconductivity in YPtBi and Related Topological Semimetals, Phys. Rev. Lett. **116**, 137001 (2016).

[4] N. P. Butch, P. Syers, K. Kirshenbaum, A. P. Hope, and J. Paglione, Superconductivity in the topological semimetal YPtBi, Phys. Rev. B **84**, 220504(R) (2011).

[5] T. V. Bay, T. Naka, Y. K. Huang, and A. de Visser, Superconductivity in noncentrosymmetric YPtBi under pressure, Phys. Rev. B **86**, 064515 (2012).

[6] H. Kim, K. Wang, Y. Nakajima, R. Hu, S. Ziemak, P. Syers, L. Wang, H. Hodovanets, J. D. Denlinger, P. M. R. Brydon, D. F. Agterberg, M. A. Tanatar, R. Prozorov, and J. Paglione, Beyond triplet: Unconventional superconductivity in a spin-3/2 topological semimetal, Sci. Adv. **4**, eaao4513 (2018).

[7] X.-C. Pan, X. Chen, H. Liu, Y. Feng, Z. Wei, Y. Zhou, Z. Chi, L. Pi, F. Yen, F. Song, X. Wan, Z. Yang, B. Wang, G. Wang, and Y. Zhang, Pressure-driven dome-shaped superconductivity and electronic structural evolution in tungsten ditelluride, Nat. Commun. **6**, 7805 (2015).

[8] D. Kang, Y. Zhou, W. Yi, C. Yang, J. Guo, Y. Shi, S. Zhang, Z. Wang, C. Zhang, S. Jiang, A. Li, K. Yang, Q. Wu, G. Zhang, L. Sun, and Z. Zhao, Superconductivity emerging from a suppressed large magnetoresistant state in tungsten ditelluride, Nat. Commun. **6**, 7804 (2015).

[9] P. Lu, J.-S. Kim, J. Yang, H. Gao, J. Wu, D. Shao, B. Li, D. Zhou, J. Sun, D. Akinwande, D. Xing, and J.-F. Lin, Origin of superconductivity in the Weyl semimetal WTe_2 under pressure, Phys. Rev. B **94**, 224512 (2016).

[10] Y. T. Chan, P. L. Alireza, K. Y. Yip, Q. Niu, K. T. Lai, and S. K. Goh, Nearly isotropic superconductivity in the layered Weyl semimetal WTe_2 at 98.5 kbar, Phys. Rev. B **96**, 180504(R) (2017).

[11] Y. Qi, P. G. Naumov, M. N. Ali, C. R. Rajamathi, W. Schnelle, O. Barkalov, M. Hanfland, S.-C. Wu, C. Shekhar, Y. Sun, V. Süß, M. Schmidt, U. Schwarz, E. Pippel, P. Werner, R. Hillebrand, T. Förster, E. Kampert, S. Parkin, R. J. Cava *et al.*, Superconductivity in Weyl semimetal candidate $MoTe_2$, Nat. Commun. **7**, 11038 (2016).

[12] D. Rhodes, R. Schönemann, N. Aryal, Q. Zhou, Q. R. Zhang, E. Kampert, Y.-C. Chiu, Y. Lai, Y. Shimura, G. T. McCandless, J. Y. Chan, D. W. Paley, J. Lee, A. D. Finke, J. P. C. Ruff, S. Das, E. Manousakis, and L. Balicas, Bulk Fermi surface of the

Weyl type-II semimetallic candidate γ-$MoTe_2$, Phys. Rev. B **96**, 165134 (2017).

[13] Y. J. Hu, Y. T. Chan, K. T. Lai, K. O. Ho, X. Guo, H.-P. Sun, K. Y. Yip, D. H. L. Ng, H.-Z. Lu, and S. K. Goh, Angular dependence of the upper critical field in the high-pressure $1T'$ phase of $MoTe_2$, Phys. Rev. Mater. **3**, 034201 (2019).

[14] Y. J. Hu, W. C. Yu, K. T. Lai, D. Sun, F. F. Balakirev, W. Zhang, J. Y. Xie, K. Y. Yip, E. I. P. Aulestia, R. Jha, R. Higashinaka, T. D. Matsuda, Y. Yanase, Y. Aoki, and S. K. Goh, Detection of Hole Pockets in the Candidate Type-II Weyl Semimetal $MoTe_2$ from Shubnikov–De Haas Quantum Oscillations, Phys. Rev. Lett. **124**, 076402 (2020).

[15] M. Sato and Y. Ando, Topological superconductors: A review, Rep. Prog. Phys. **80**, 076501 (2017).

[16] Y. Li and Z.-A. Xu, Exploring topological superconductivity in topological materials, Adv. Quant. Technol. **2**, 1800112 (2019).

[17] A. A. Soluyanov, D. Gresch, Z. Wang, Q. Wu, M. Troyer, X. Dai, and B. A. Bernevig, Type-II Weyl semimetals, Nature (Lond.) **527**, 495 (2015).

[18] K. Deng, G. Wan, P. Deng, K. Zhang, S. Ding, E. Wang, M. Yan, H. Huang, H. Zhang, Z. Xu, J. Denlinger, A. Fedorov, H. Yang, W. Duan, H. Yao, Y. Wu, S. Fan, H. Zhang, X. Chen, and S. Zhou, Experimental observation of topological Fermi arcs in type-II Weyl semimetal $MoTe_2$, Nat. Phys. **12**, 1105 (2016).

[19] L. Huang, T. M. McCormick, M. Ochi, Z. Zhao, M.-T. Suzuki, R. Arita, Y. Wu, D. Mou, H. Cao, J. Yan, N. Trivedi, and A. Kaminski, Spectroscopic evidence for a type II Weyl semimetallic state in $MoTe_2$, Nat. Mater. **15**, 1155 (2016).

[20] J. Jiang, Z. K. Liu, Y. Sun, H. F. Yang, C. R. Rajamathi, Y. P. Qi, L. X. Yang, C. Chen, H. Peng, C.-C. Hwang, S. Z. Sun, S.-K. Mo, I. Vobornik, J. Fujii, S. S. P. Parkin, C. Felser, B. H. Yan, and Y. L. Chen, Signature of type-II Weyl semimetal phase in $MoTe_2$, Nat. Commun. **8**, 13973 (2017).

[21] W. Wang, S. Kim, M. Liu, F. A. Cevallos, R. J. Cava, and N. P. Ong, Evidence for an edge supercurrent in the Weyl superconductor $MoTe_2$, Science **368**, 534 (2020).

[22] H. Takahashi, T. Akiba, K. Imura, T. Shiino, K. Deguchi, N. K. Sato, H. Sakai, M. S. Bahramy, and S. Ishiwata, Anticorrelation between polar lattice instability and superconductivity in the Weyl semimetal candidate $MoTe_2$, Phys. Rev. B **95**, 100501(R) (2017).

[23] C. Heikes, I.-L. Liu, T. Metz, C. Eckberg, P. Neves, Y. Wu, L. Hung, P. Piccoli, H. Cao, J. Leao, J. Paglione, T. Yildirim, N. P. Butch, and W. Ratcliff, Mechanical control of crystal symmetry and superconductivity in Weyl semimetal $MoTe_2$, Phys. Rev. Mater. **2**, 074202 (2018).

[24] S. Lee, J. Jang, S.-I. Kim, S.-G. Jung, J. Kim, S. Cho, S. W. Kim, J. Y. Rhee, K.-S. Park, and T. Park, Origin of extremely large magnetoresistance in the candidate type-II Weyl semimetal $MoTe_{2-x}$, Sci. Rep. **8**, 13937 (2018).

[25] Z. Guguchia, F. von Rohr, Z. Shermadini, A. T. Lee, S. Banerjee, A. R. Wieteska, C. A. Marianetti, B. A. Frandsen, H. Luetkens, Z. Gong, S. C. Cheung, C. Baines, A. Shengelaya, G. Taniashvili, A. N. Pasupathy, E. Morenzoni, S. J. L. Billinge, A. Amato, R. J. Cava, R. Khasanov *et al.*, Signatures of the topological s^{+-} superconducting order parameter in the type-II Weyl semimetal T_d-$MoTe_2$, Nat. Commun. **8**, 1082 (2017).

[26] F. C. Chen, X. Luo, R. C. Xiao, W. J. Lu, B. Zhang, H. X. Yang, J. Q. Li, Q. L. Pei, D. F. Shao, R. R. Zhang, L. S. Ling, C. Y. Xi, W. H. Song, and Y. P. Sun, Superconductivity enhancement in the S-doped Weyl semimetal candidate $MoTe_2$, Appl. Phys. Lett. **108**, 162601 (2016).

[27] S. Cho, S. H. Kang, H. S. Yu, H. W. Kim, W. Ko, S. W. Hwang, W. H. Han, D.-H. Choe, Y. H. Jung, K. J. Chang, Y. H. Lee, H. Yang, and S. W. Kim, Te vacancy-driven superconductivity in orthorhombic molybdenum ditelluride, 2D Mater. **4**, 021030 (2017).

[28] M. Mandal, S. Marik, K. P. Sajilesh, Arushi, D. Singh, J. Chakraborty, N. Ganguli, and R. P. Singh, Enhancement of the superconducting transition temperature by Re doping in Weyl semimetal $MoTe_2$, Phys. Rev. Mater. **2**, 094201 (2018).

[29] R. Dahal, L. Z. Deng, N. Poudel, M. Gooch, Z. Wu, H. C. Wu, H. D. Yang, C. K. Chang, and C. W. Chu, Tunable structural phase transition and superconductivity in the Weyl semimetal $Mo_{1-x}W_xTe_2$, Phys. Rev. B **101**, 140505(R) (2020).

[30] D. A. Rhodes, A. Jindal, N. F. Q. Yuan, Y. Jung, A. Antony, H. Wang, B. Kim, Y.-c. Chiu, T. Taniguchi, K. Watanabe, K. Barmak, L. Balicas, C. R. Dean, X. Qian, L. Fu, A. N. Pasupathy, and J. Hone, Enhanced superconductivity in monolayer T_d-$MoTe_2$, Nano Lett. **21**, 2505 (2021).

[31] K. Ikeura, H. Sakai, M. S. Bahramy, and S. Ishiwata, Rich structural phase diagram and thermoelectric properties of layered tellurides $Mo_{1-x}Nb_xTe_2$, APL Mater. **3**, 041514 (2015).

[32] H. Sakai, K. Ikeura, M. S. Bahramy, N. Ogawa, D. Hashizume, J. Fujioka, Y. Tokura, and S. Ishiwata, Critical enhancement of thermopower in a chemically tuned polar semimetal $MoTe_2$, Sci. Adv. **2**, e1601378 (2016).

[33] See Supplemental Material at http://link.aps.org/supplemental/10.1103/PhysRevMaterials.7.084802 for the representative EDX spectrum with all doped samples, the raw data of Hall resistivity ρ_{xy} of all doping levels, from which we extracted R_H, and the $d\rho(T)/dT$ data on cooling or warming for determination of T_s

[34] T. Zandt, H. Dwelk, C. Janowitz, and R. Manzke, Quadratic temperature dependence up to 50 K of the resistivity of metallic $MoTe_2$, J. Alloys Compd. **442**, 216 (2007).

[35] K. Y. Yip, S. T. Lam, K. H. Yu, W. S. Chow, J. Zeng, K. T. Lai, and S. K. Goh, Drastic enhancement of the superconducting temperature in type-II Weyl semimetal candidate $MoTe_2$ via biaxial strain, APL Mater. **11**, 021111 (2023).

[36] Q. Zhou, D. Rhodes, Q. R. Zhang, S. Tang, R. Schönemann, and L. Balicas, Hall effect within the colossal magnetoresistive semimetallic state of $MoTe_2$, Phys. Rev. B **94**, 121101(R) (2016).

[37] N. P. Armitage, P. Fournier, and R. L. Greene, Progress and perspectives on electron-doped cuprates, Rev. Mod. Phys. **82**, 2421 (2010).

[38] B. Keimer, S. A. Kivelson, M. R. Norman, S. Uchida, and J. Zaanen, From quantum matter to high-temperature superconductivity in copper oxides, Nature (Lond.) **518**, 179 (2015).

[39] Y. Zhang, F. Fei, R. Liu, T. Zhu, B. Chen, T. Qiu, Z. Zuo, J. Guo, W. Tang, L. Zhou *et al.*, Enhanced superconductivity and upper critical field in Ta-doped Weyl semimetal T_d-$MoTe_2$, Adv. Mater. **35**, 2207841 (2023).